

Supplementary Information

Ingenious double-modified strategy to prepare “hexagonal warrior” separator for lithium metal batteries

Shitong Sun, Bo Jin,* Hui Liu, Qing Jiang

Key Laboratory of Automobile Materials, Ministry of Education, and School of Materials Science and Engineering, Jilin University, Changchun 130022, China

* Corresponding author. E-mail: jinbo@jlu.edu.cn (B. Jin)

Supplementary Figures

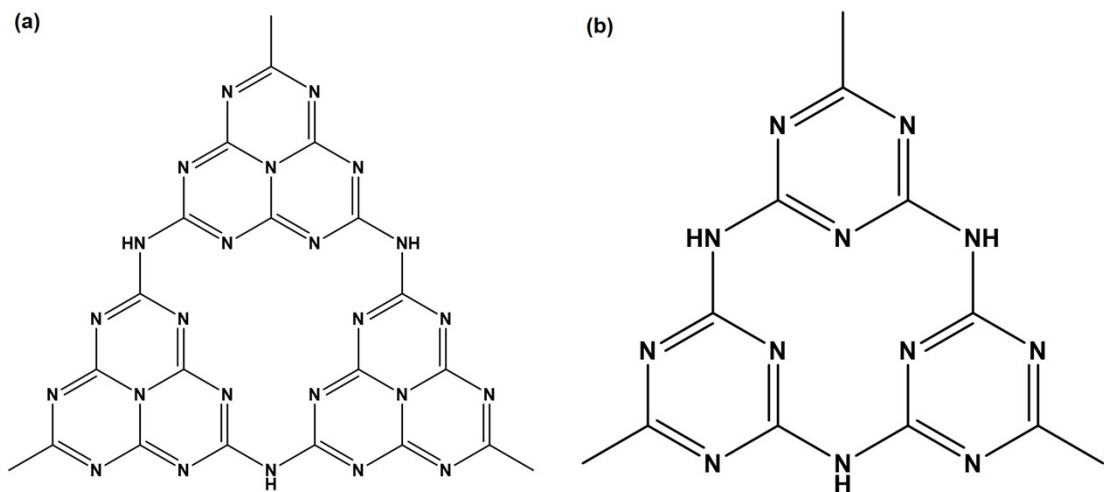


Figure S1 Structural charts of (a) heptazine-based CN and (b) triazine-based CN.

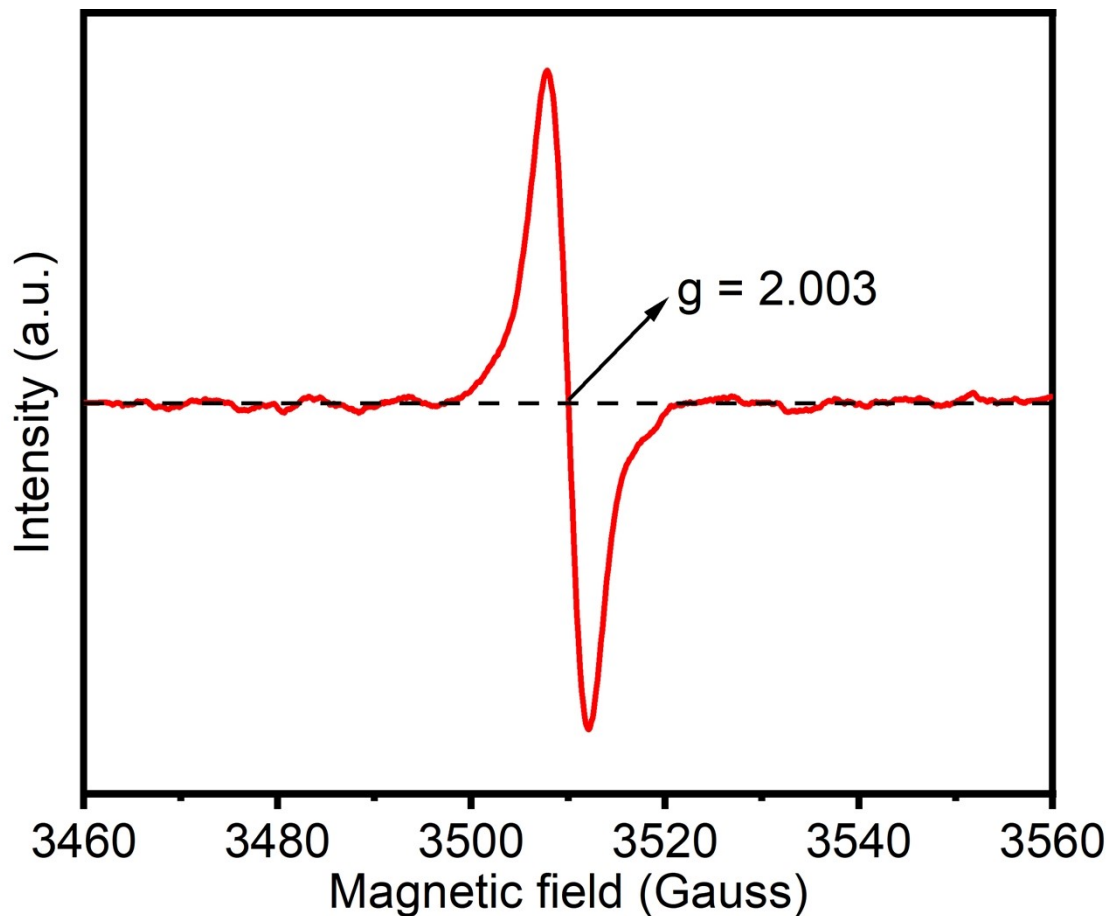


Figure S2 EPR spectrum of CoMo-LDH.

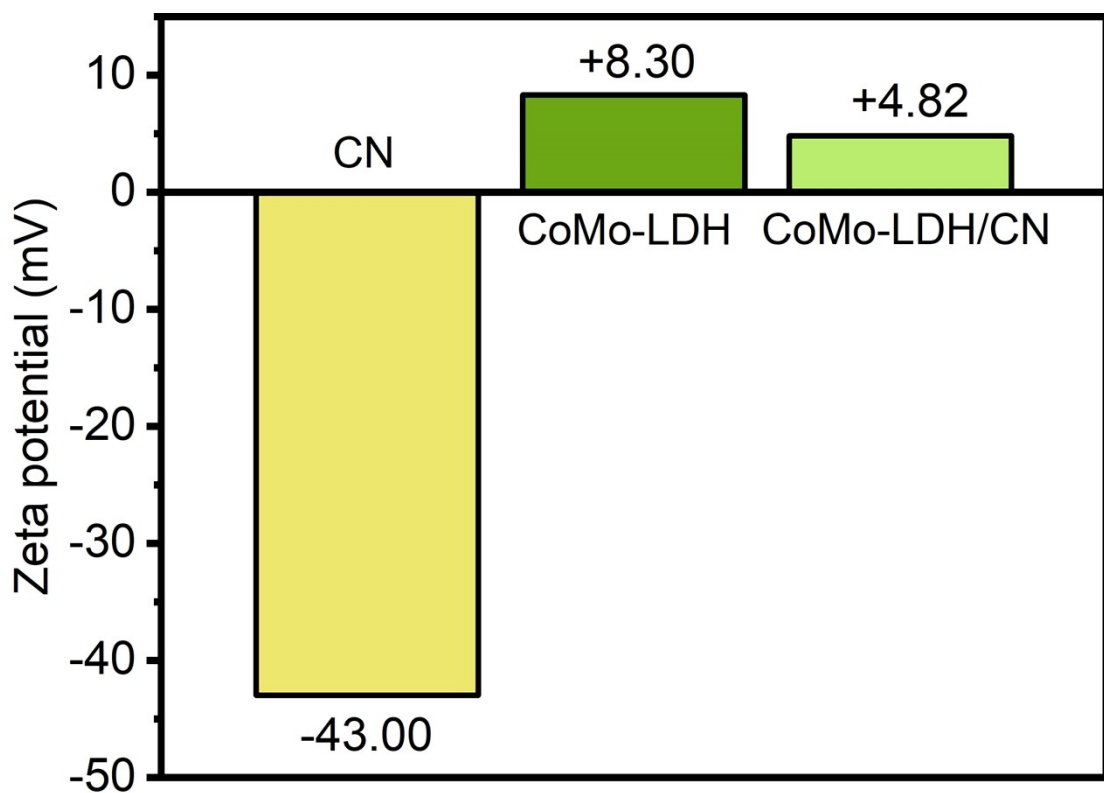


Figure S3 Histograms of zeta potential of CN, CoMo-LDH, and CoMo-LDH/CN.

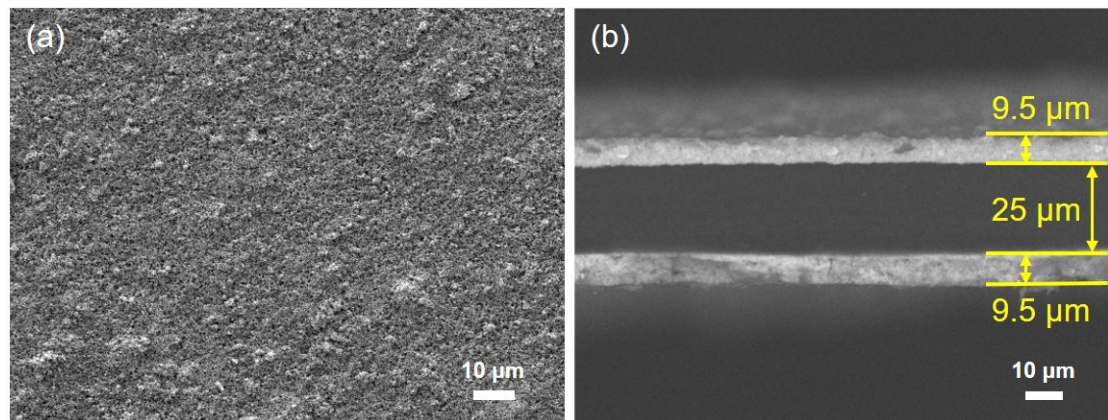


Figure S4 (a) The surface and (b) cross-sectional SEM images of DMP separator.

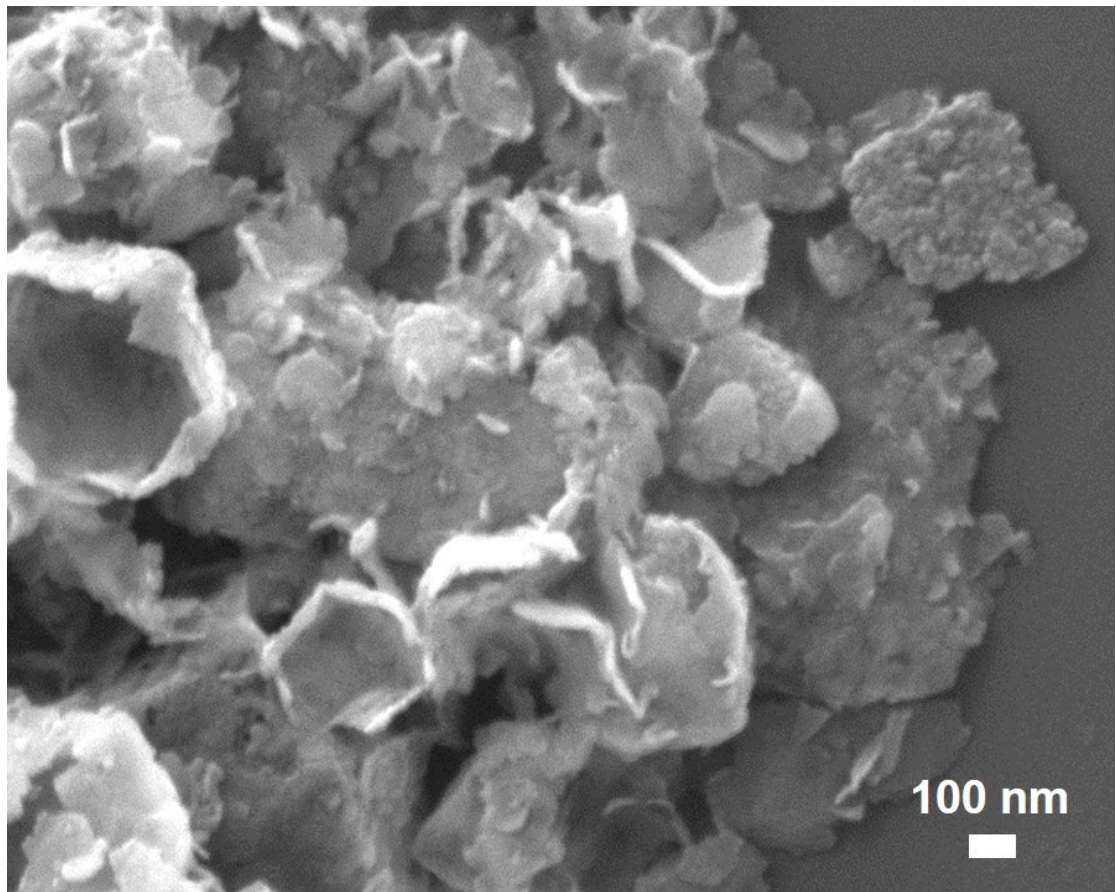


Figure S5 SEM image of CoMo-LDH/CN.

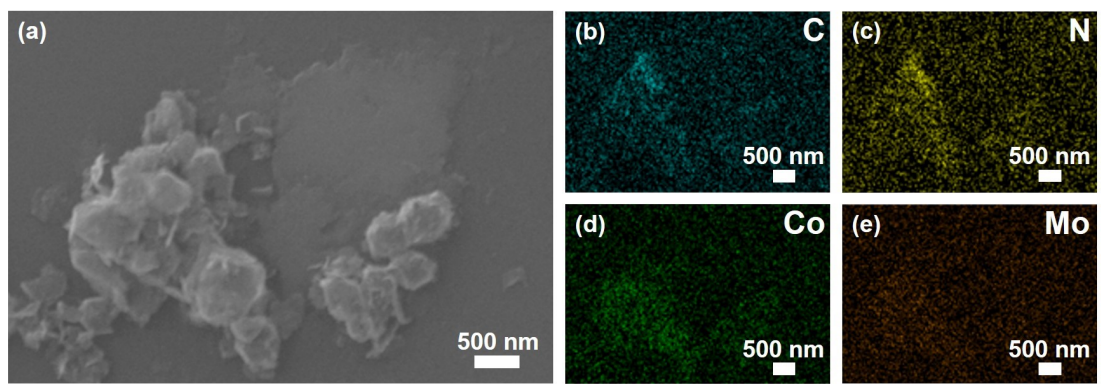


Figure S6 (a) SEM image and (b-e) corresponding C, N, Co, and Mo elemental mappings of CoMo-LDH/CN.

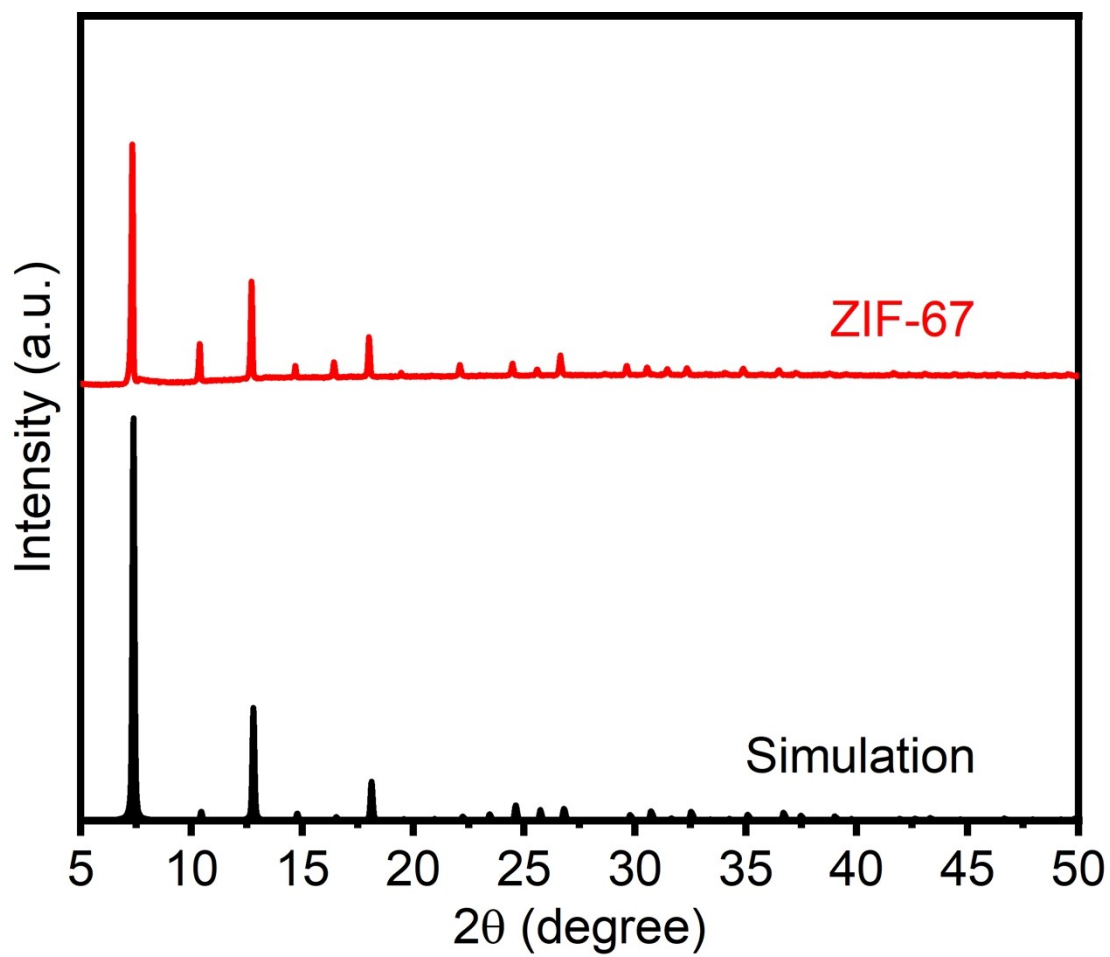


Figure S7 XRD pattern of ZIF-67.

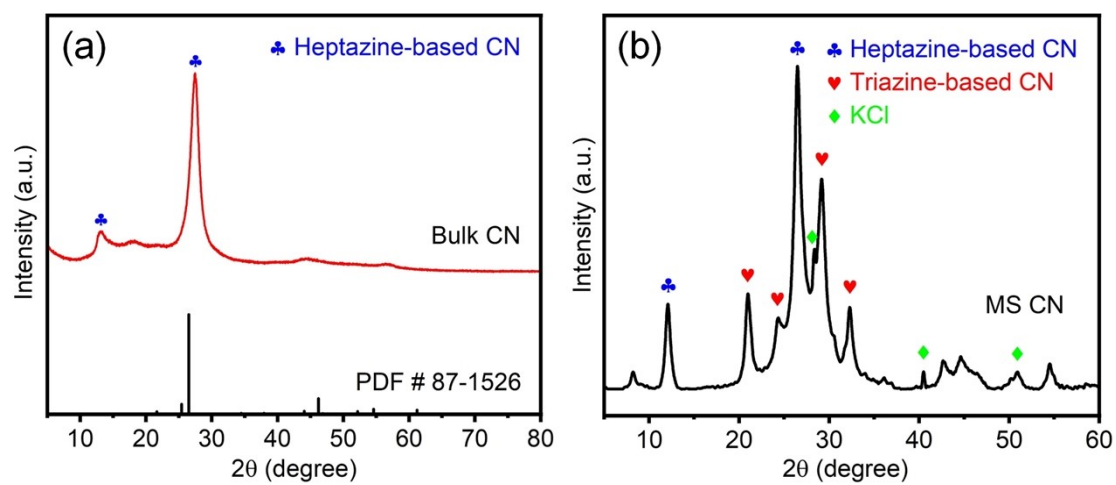


Figure S8 XRD patterns of (a) bulk CN and (b) MS CN.

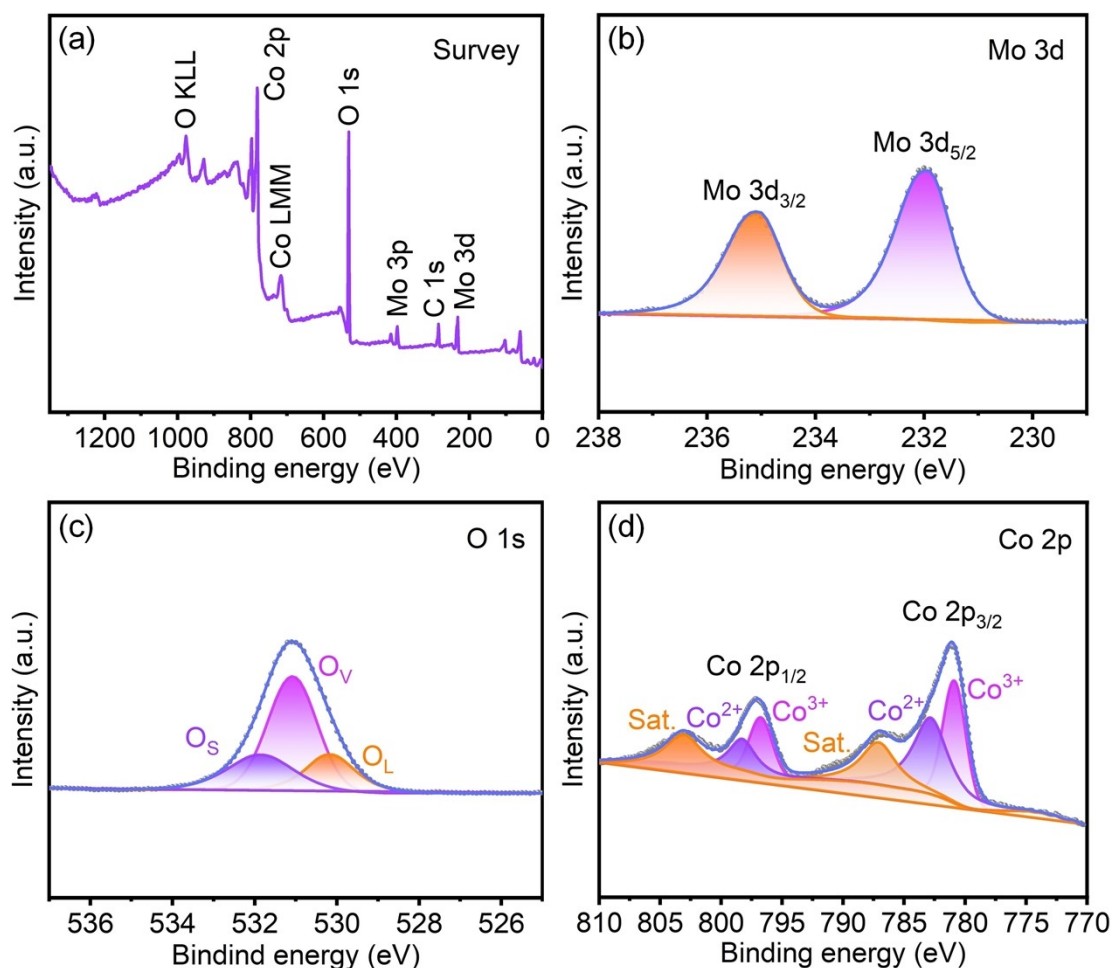


Figure S9 (a) XPS survey spectrum of CoMo-LDH. High-resolution XPS spectra of (b) Mo 3d, (c) O 1s, and (d) Co 2p in CoMo-LDH.

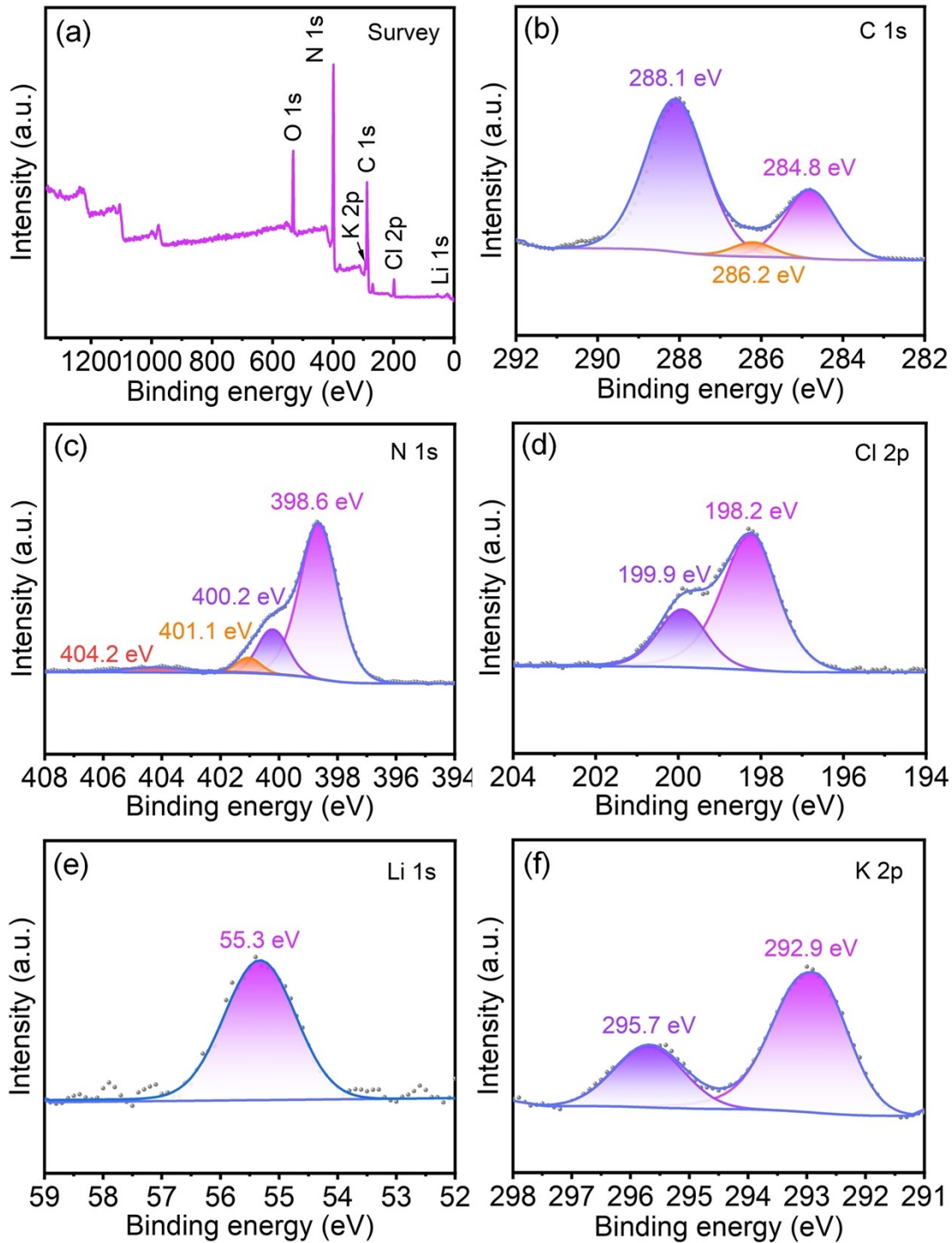


Figure S10 (a) XPS survey spectrum of MS CN. High-resolution XPS spectra of (b) C 1s, (c) N 1s, (d) Cl 2p, (e) Li 1s, and (f) K 2p in MS CN.

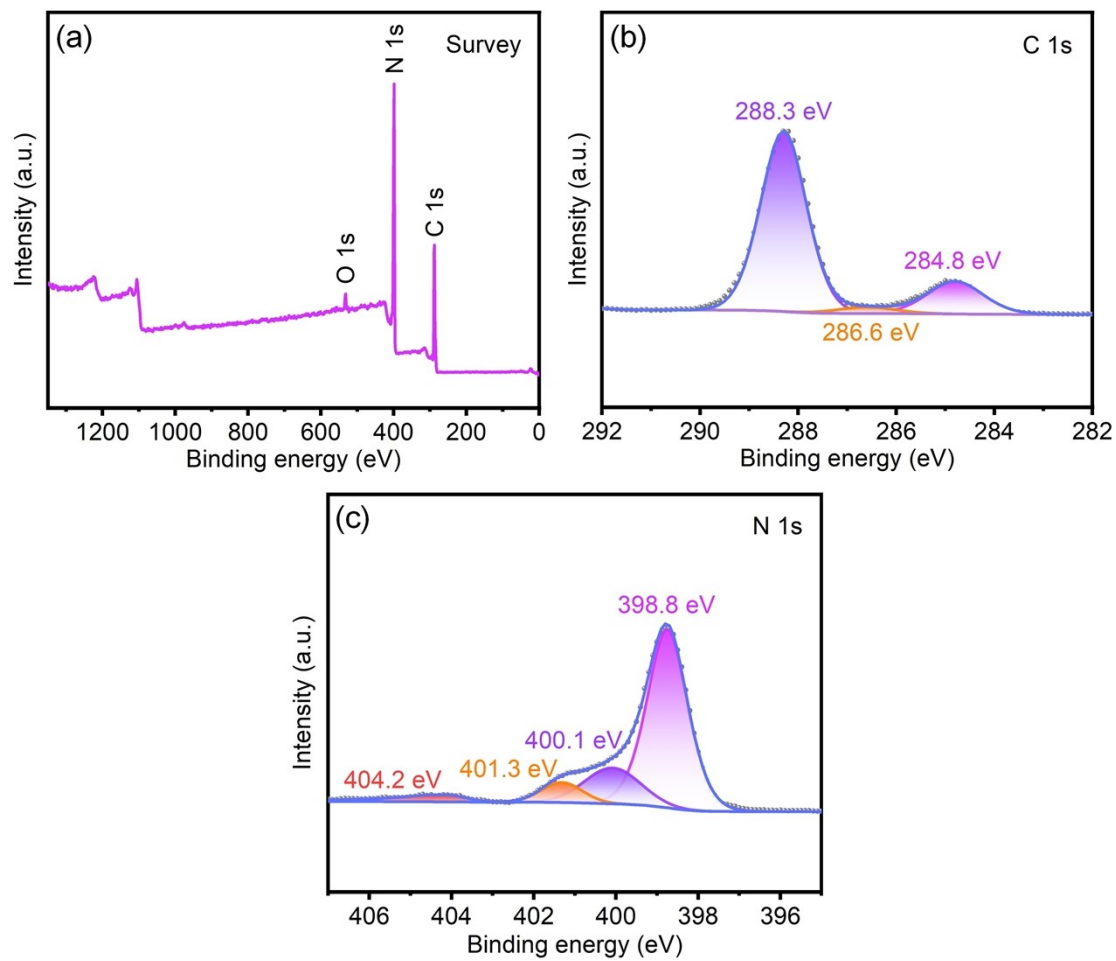


Figure S11 (a) XPS survey spectrum of bulk CN. High-resolution XPS spectra of (b) C 1s and (c) N 1s of bulk CN.

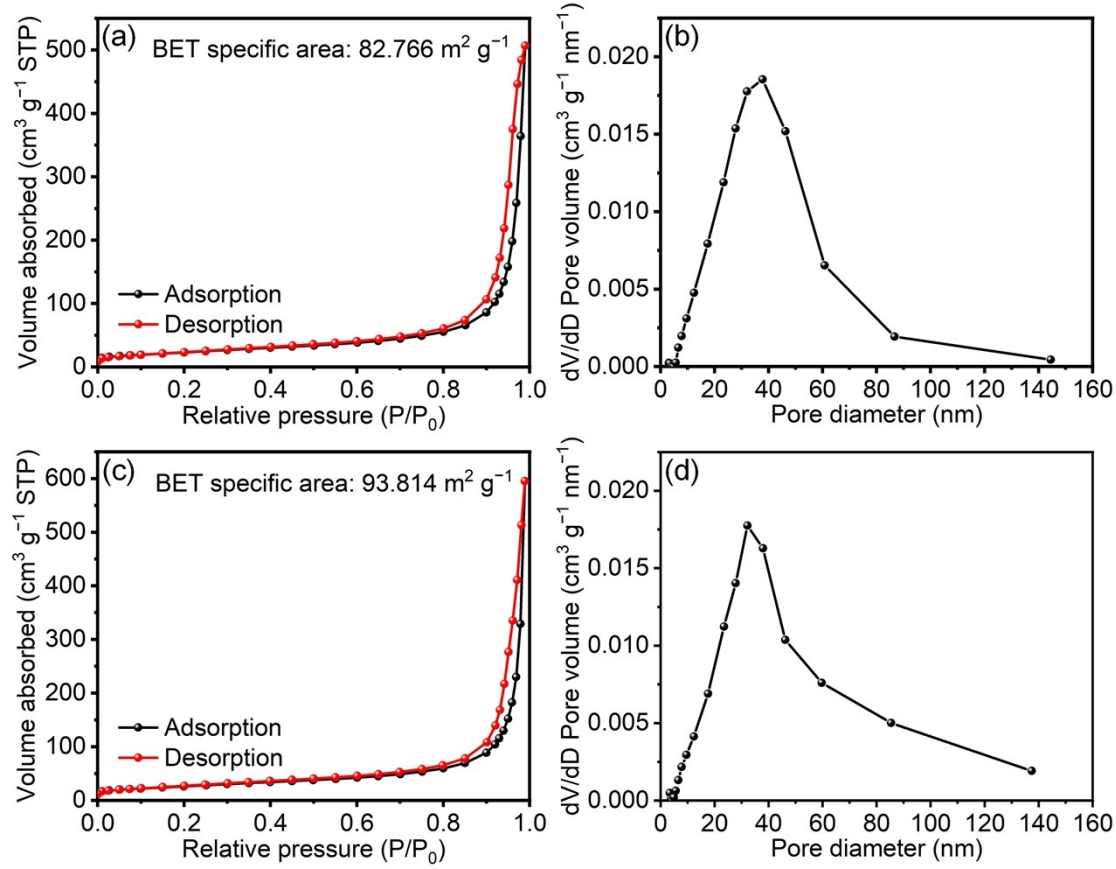


Figure S12 Nitrogen absorption-desorption isotherms and corresponding pore size distribution curves of (a, b) CoMo-LDH/CN and (c, d) CoMo-LDH.

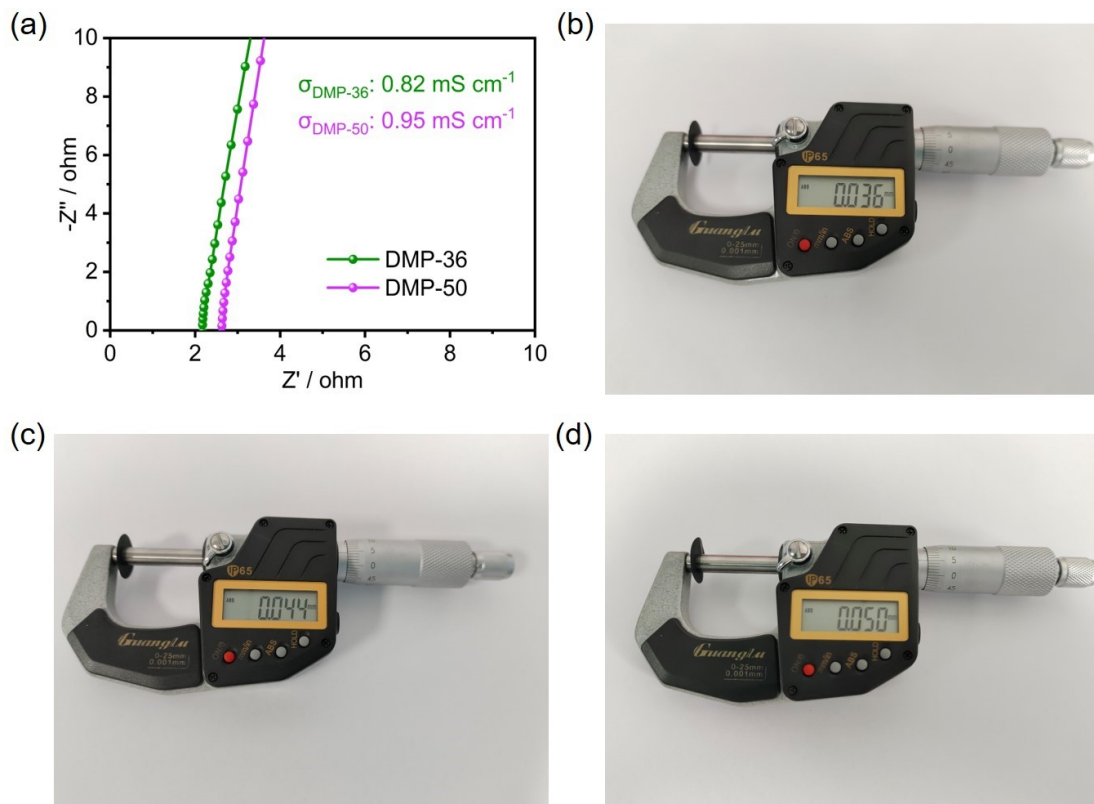


Figure S13 (a) EIS spectra of DMP-36 and DMP-50 separators. Optical pictures of actual thickness of (b) DMP-36, (c) DMP, and (d) DMP-50 separators.

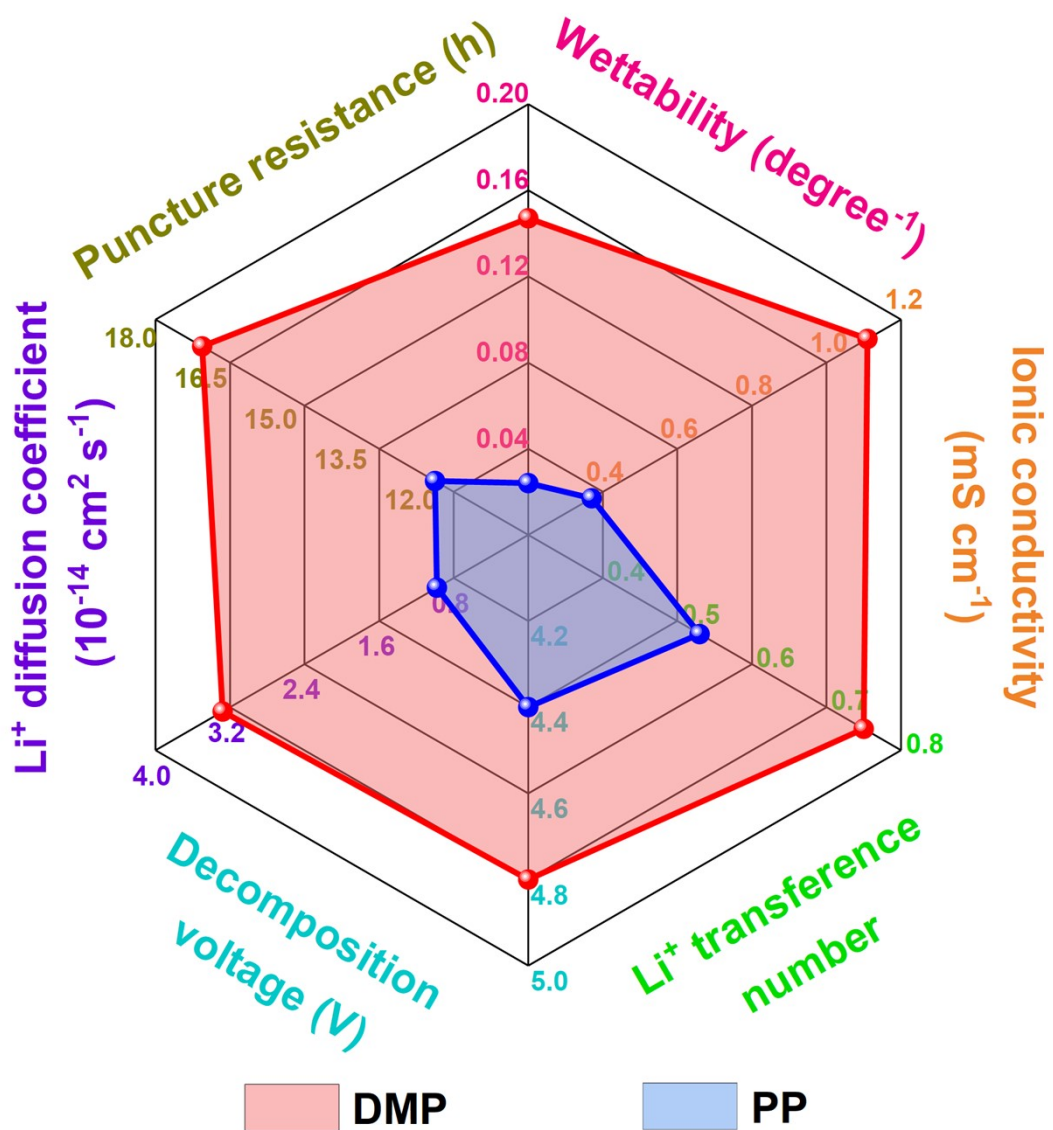


Figure S14 Comparison of various properties of DMP and PP separators.

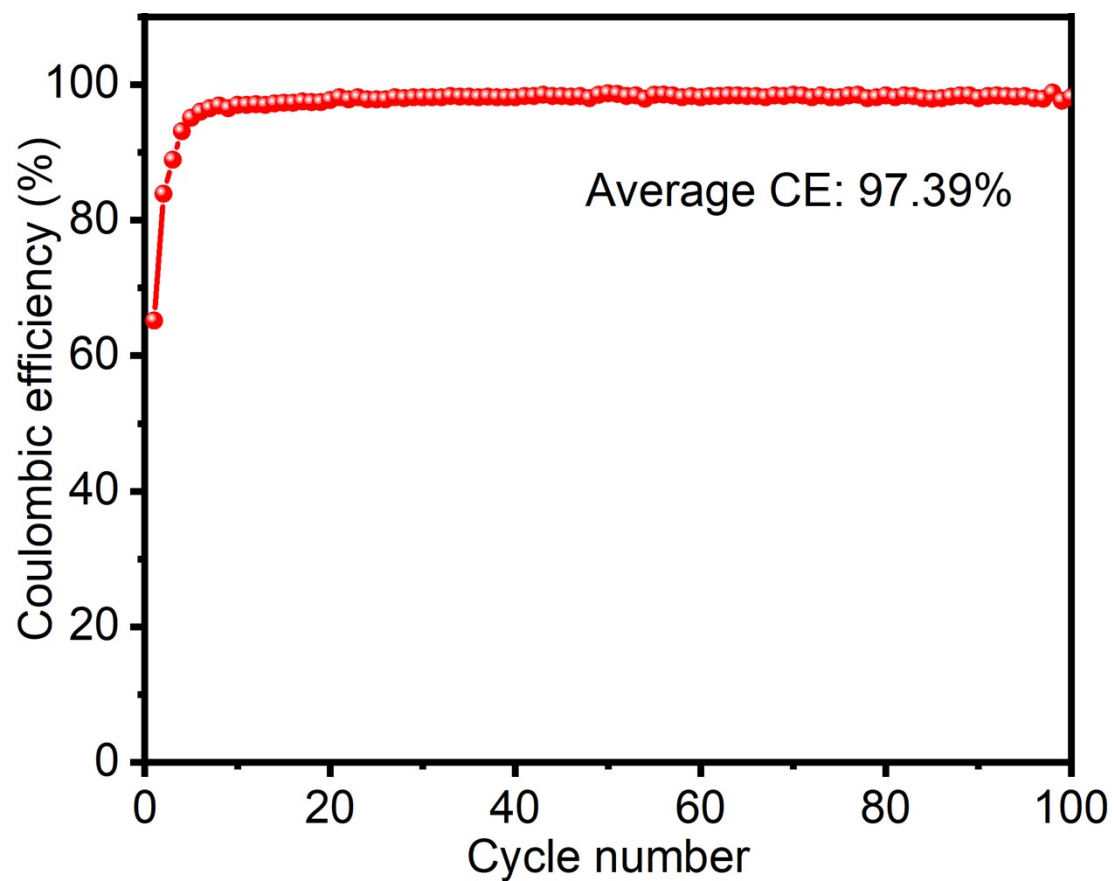


Figure S15 CE of Li//Cu half-cell at $0.5 \text{ mA cm}^{-2}/1 \text{ mAh cm}^{-2}$.

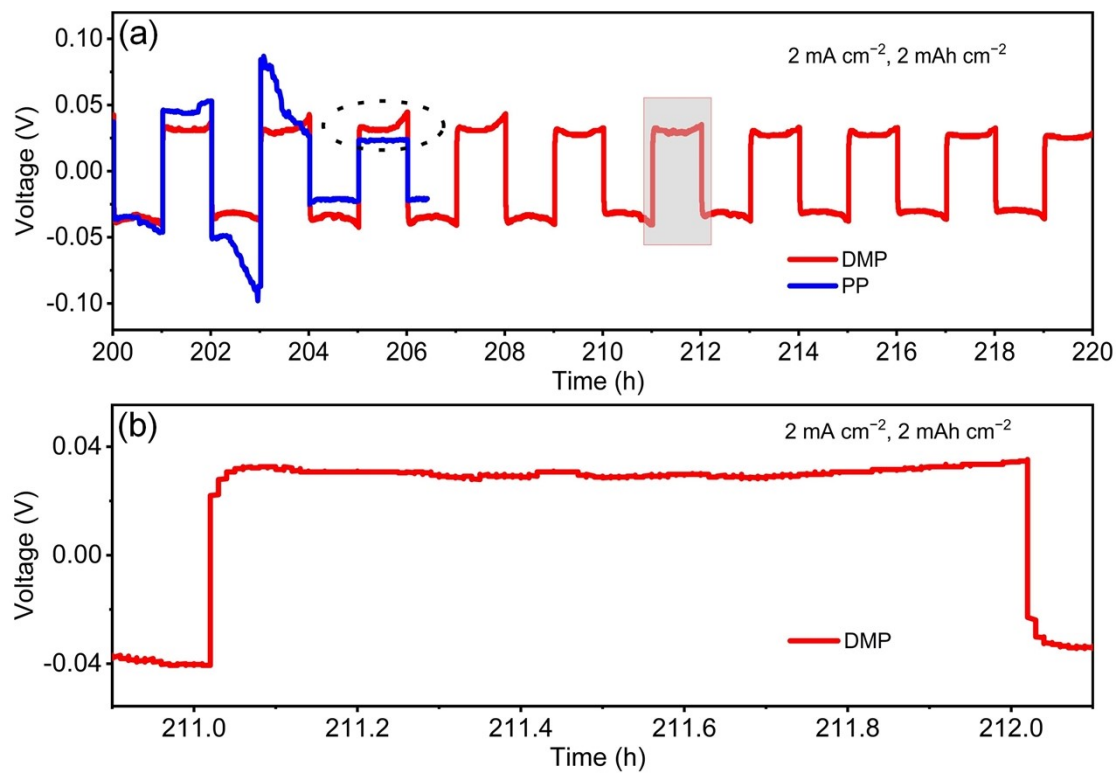


Figure S16 (a, b) Partial magnification of voltage-time profiles at $2 \text{ mA cm}^{-2}/2 \text{ mAh cm}^{-2}$ in Figure 4f.

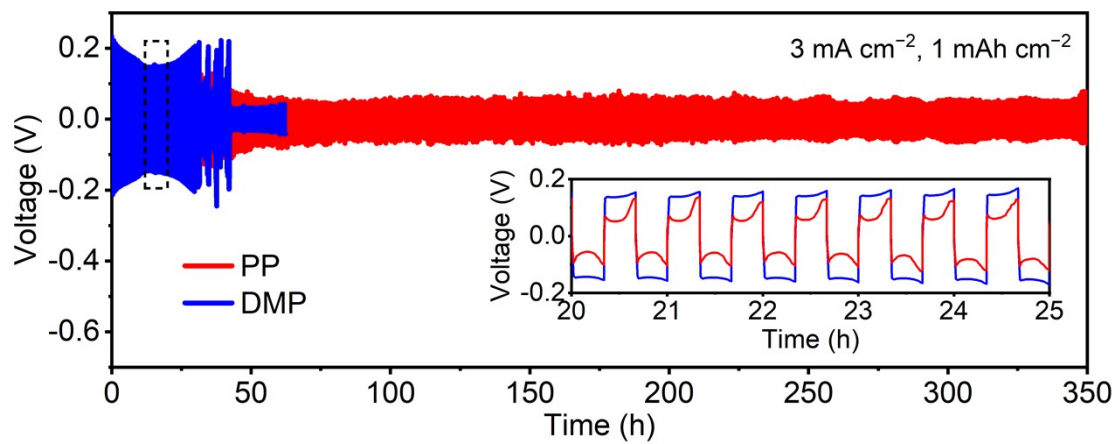


Figure S17 Voltage-time profiles of Li//Li symmetric cells with PP and DMP at $3 \text{ mA cm}^{-2}/1 \text{ mAh cm}^{-2}$.

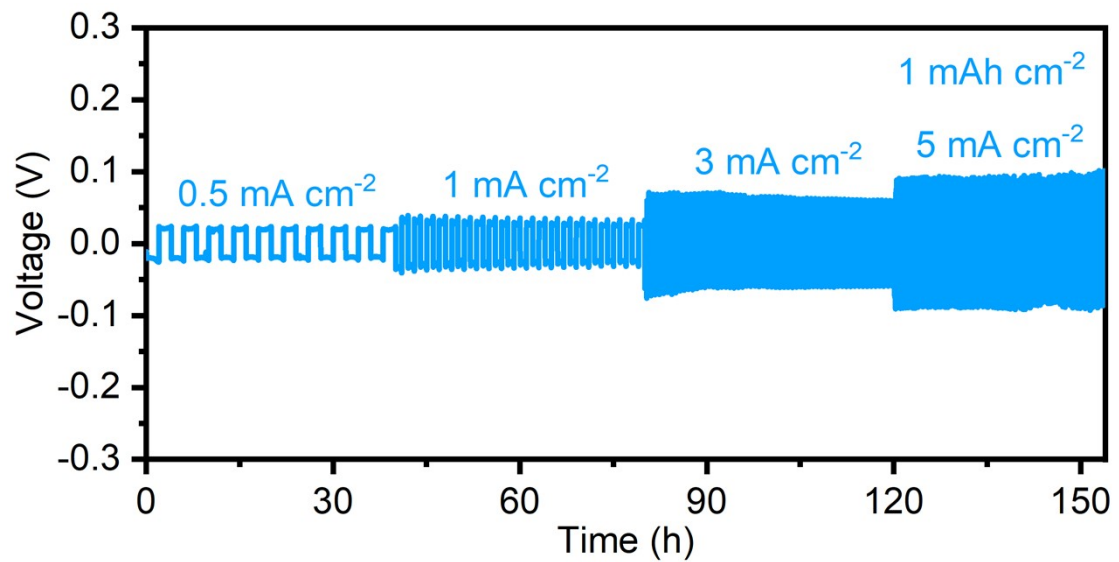


Figure S18 Rate performance of Li//Li symmetric cell with DMP separator at 0.5 to 5 mA cm^{-2} and area specific capacity of 1 mAh cm^{-2} .

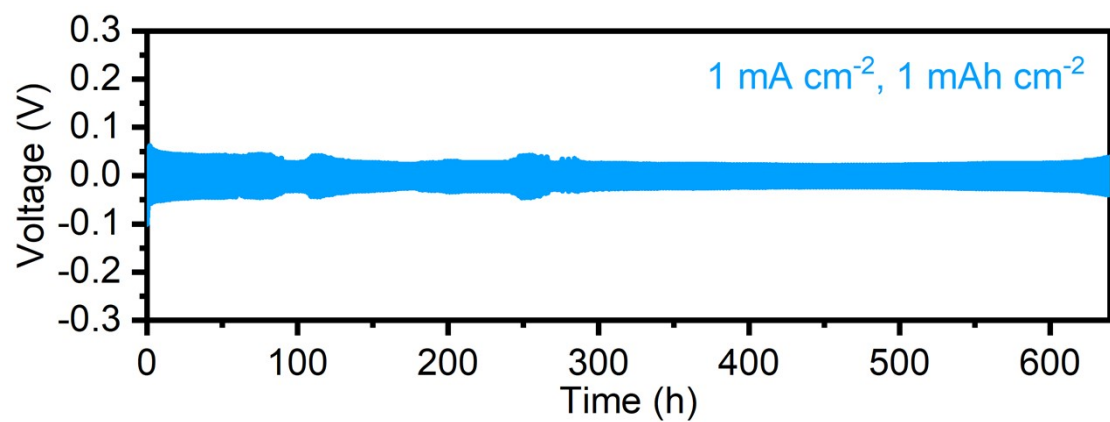


Figure S19 Voltage-time profile of Li//Li symmetric cell with DMP separator at 1 $\text{mA cm}^{-2}/\text{1 mAh cm}^{-2}$ in ester electrolyte.

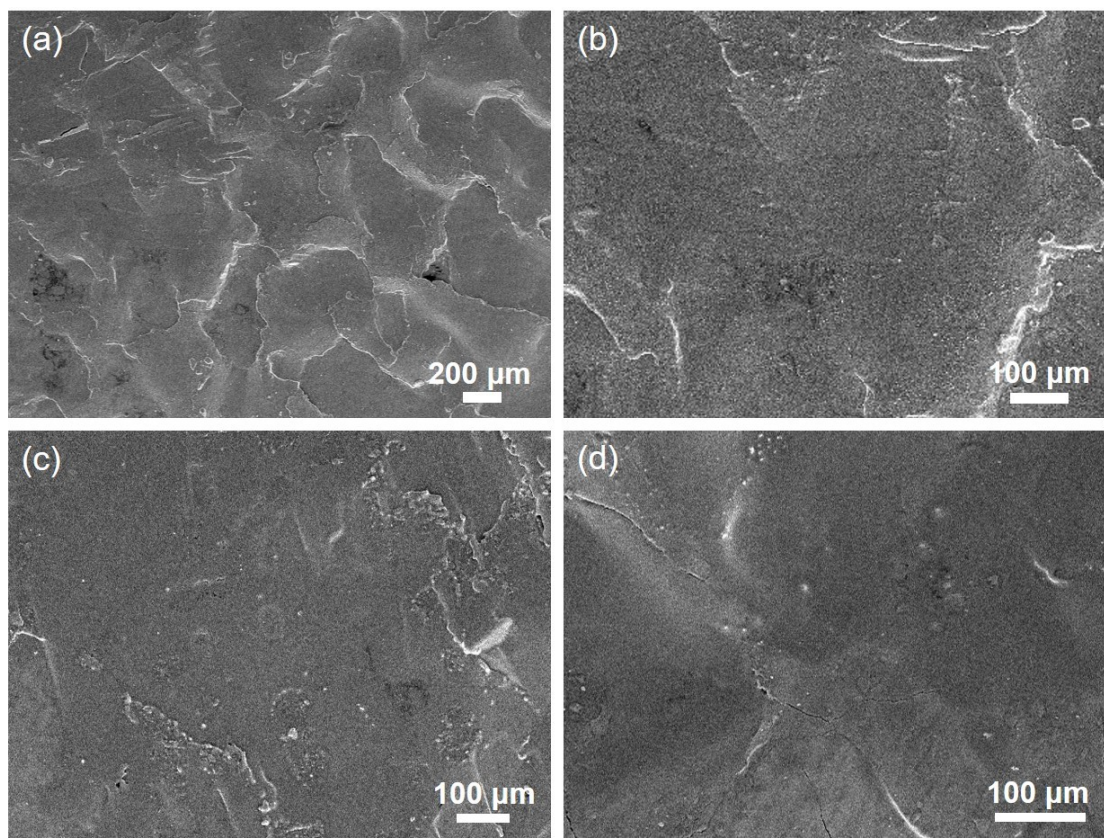


Figure S20 SEM images of Li foils derived from Li//Li symmetric cell at 1 mA cm^{-2} with area specific capacities of (a, b) 1 mAh cm^{-2} , (c) 3 mAh cm^{-2} , and (d) 5 mAh cm^{-2} .

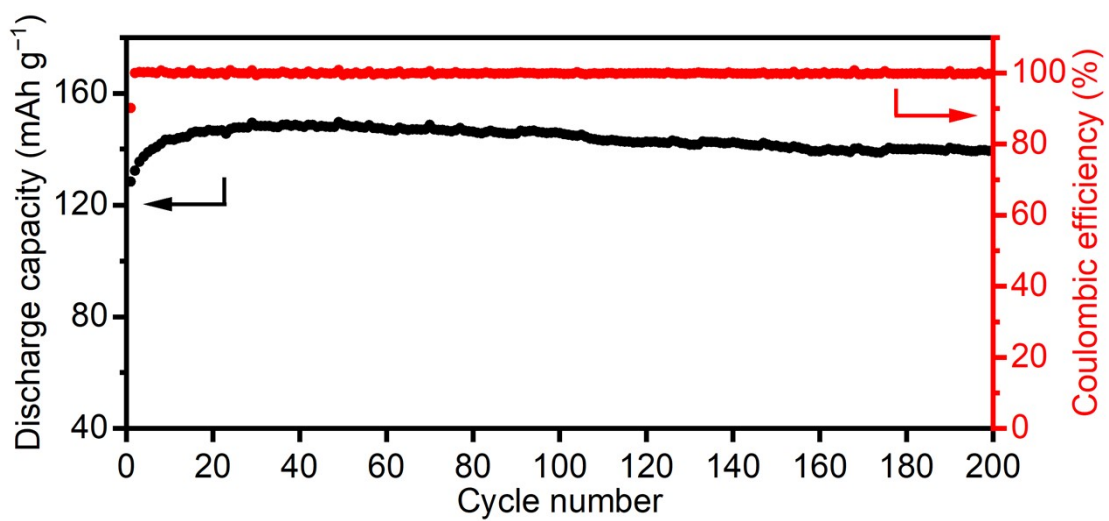


Figure S21 Cycling performance of Li//LFP full-cell with DMP separator at 0.5 C.

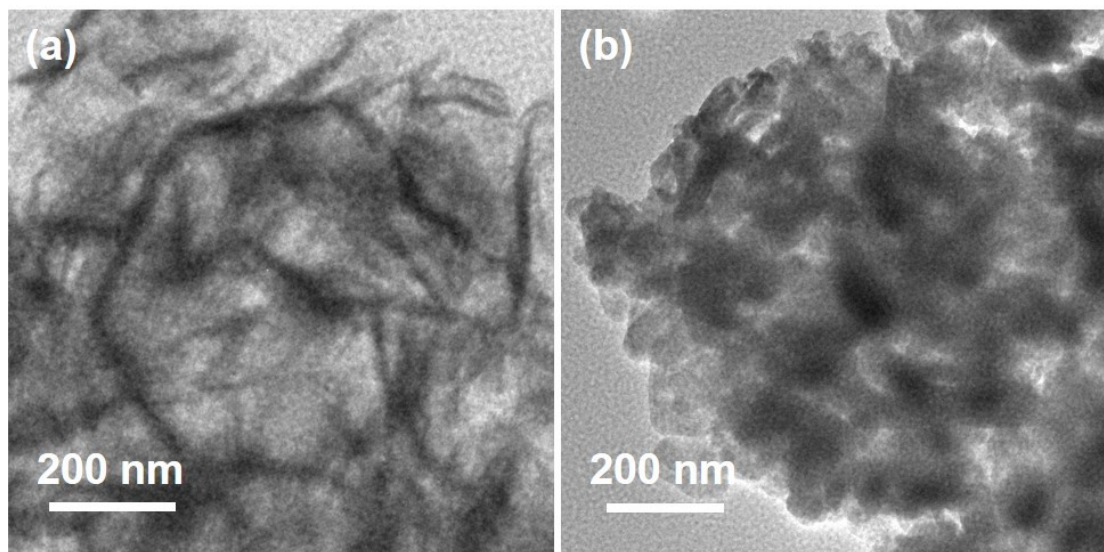


Figure S22 TEM images of CoMo-LDH/CN (a) before cycling and (b) after cycles.

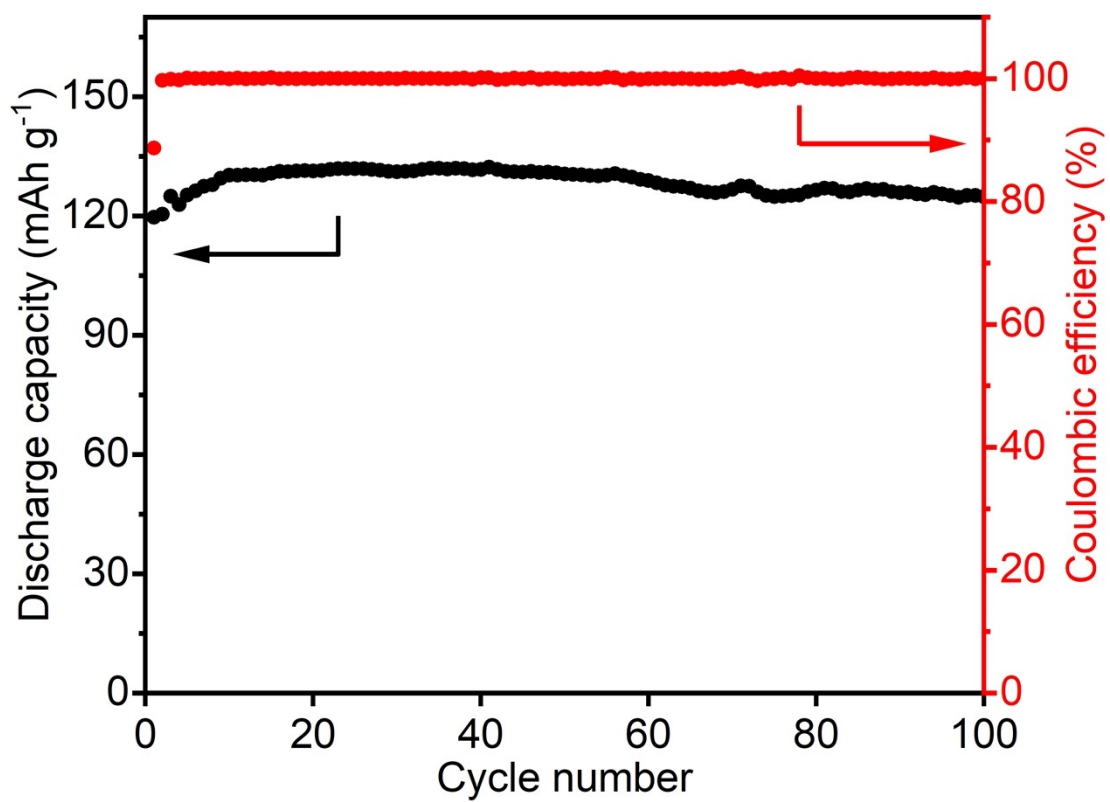


Figure S23 Cycling performance of Li//LFP full-cell with DMP separator at 1 C. The mass loading of LFP is 5.5 mg cm^{-2} .

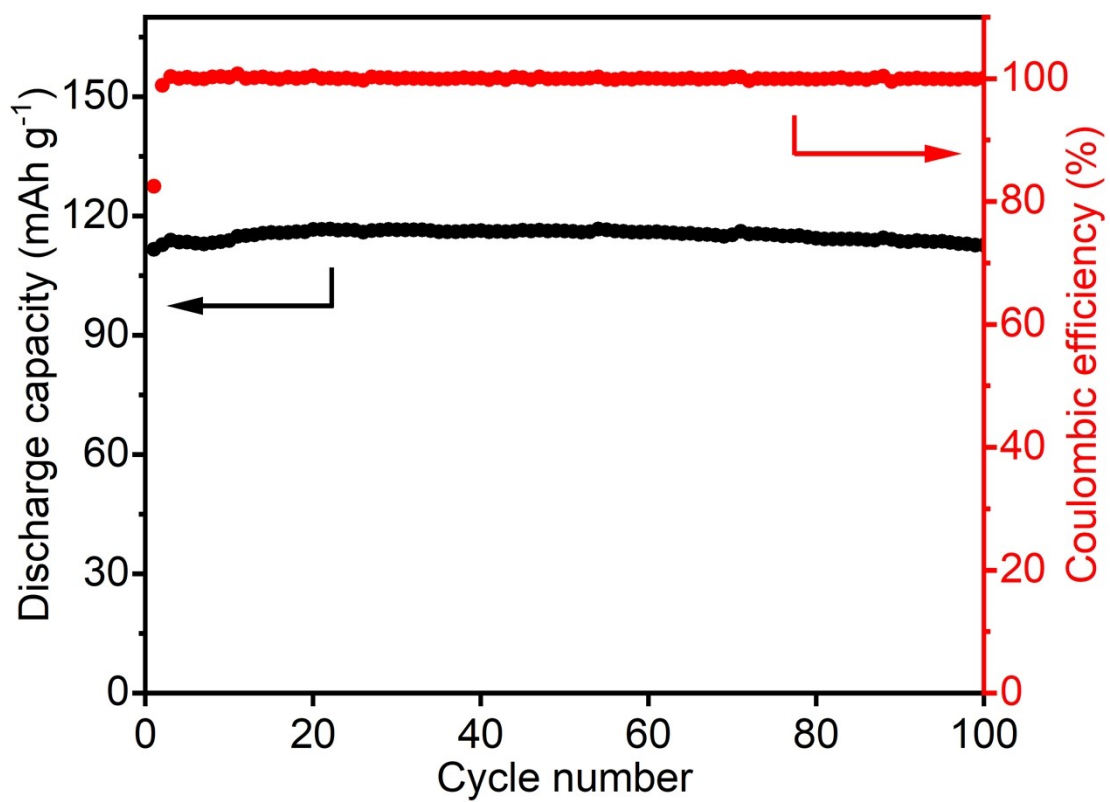


Figure S24 Cycling performance of Li//LFP full-cell with DMP separator at 1 C. The thickness of Li metal is 0.23 mm, and the mass loading of LFP is 6.0 mg cm⁻².

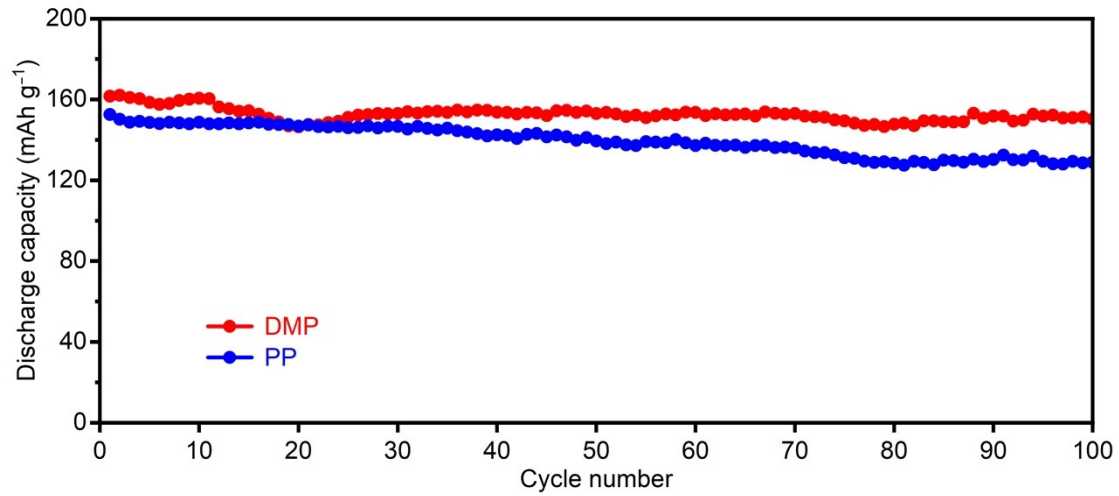


Figure S25 Cycling performance of Li//NCM523 full-cells with DMP and PP separators at 0.2 C.

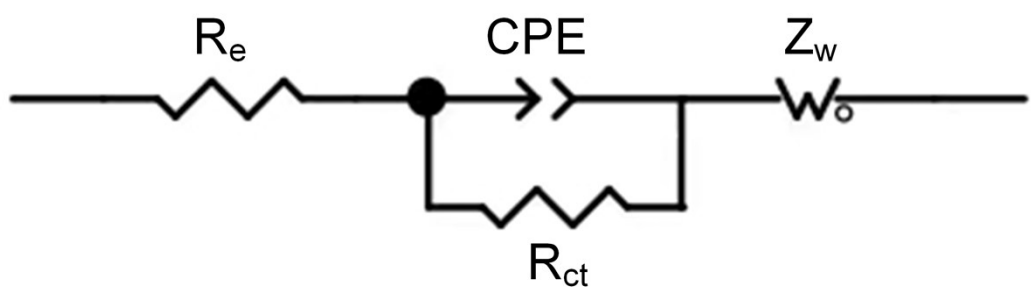


Figure S26 The corresponding equivalent circuit.

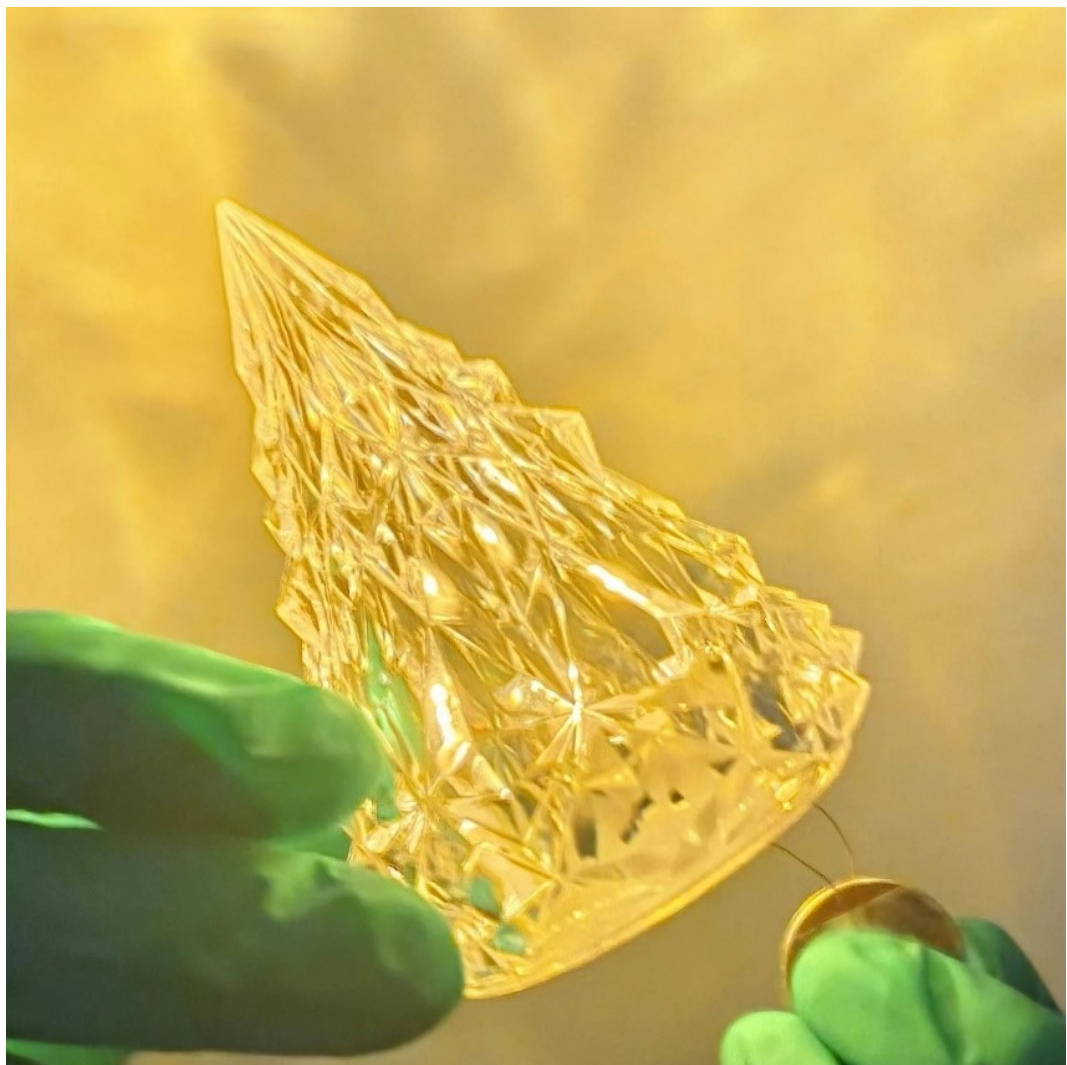


Figure S27 Iceberg lighted by Li//NCM523 full cell with DMP separator.

Table S1 Comparison of cycle life of Li/Li symmetric cells with DMP separators with other reported literatures.

Sample	Current density (mA cm ⁻²)	Area capacity (mAh cm ⁻²)	Time (h)	Ref.
BNNs@CNFs	1	1	400	S1
Ti _{0.87} O ₂ /PP	2	1	300	S2
ST@Al ₂ O ₃ -PE	1	0.5	400	S3
COF@PP	1	0.5	800	S4
SCOF-2-modified separator	1	1	350	S5
PP/LAGP+MXene	1	1	700	S6
MOFs@PP	1	0.5	150	S7
Si-PP-Si	0.5	1	1000	S8
AAPP/CB@PP@LAGP	1	1	400	S9
HP-Cu@Sn	1	1	800	S10
LiAl LDH@PP	1	1	1600	S11
rGO/Li-Al-LDH@PP	1	0.5	1100	S12
DMP	1	1	1200	This
	3	1	350	work

Notes and references

- S1 Y. J. Li, T. T. Gao, D. Y. Ni, Y. Zhou, M. Yousaf, Z. Q. Guo, J. H. Zhou, P. Zhou, Q. Wang, S. J. Guo, Two birds with one stone: Interfacial engineering of multifunctional janus separator for lithium-sulfur batteries, *Adv. Mater.*, 2022, **34**, 2107638.
- S2 P. Xiong, F. Zhang, X. Y. Zhang, Y. F. Liu, Y. Y. Wu, S. J. Wang, J. Safaei, B. Sun, R. Z. Ma, Z. W. Liu, Y. Bando, T. Sasaki, X. Wang, J. W. Zhu, G. X. Wang, Atomic-scale regulation of anionic and cationic migration in alkali metal batteries, *Nat. Commun.*, 2021, **12**, 4184.
- S3 T. T. Zhou, W. H. Tang, J. W. Lv, Y. R. Deng, Q. Liu, L. Zhang, R. P. Liu, Yolk-shell structured ST@Al₂O₃ enables functional PE separator with enhanced Lewis acid sites for high-performance lithium metal batteries, *Small*, 2023, **19**, 2303924.
- S4 C. Wang, W. Z. Li, Y. H. Jin, J. B. Liu, H. Wang, Q. Q. Zhang, Functional separator enabled by covalent organic frameworks for high-performance Li metal batteries, *Small*, 2023, **19**, 2300023.
- S5 J. Xu, S. H. An, X. Y. Song, Y. J. Cao, N. Wang, X. Qiu, Y. Zhang, J. W. Chen, X. L. Duan, J. H. Huang, W. Li, Y. G. Wang, Towards high performance Li-S batteries via sulfonate-rich COF-modified separator, *Adv. Mater.*, 2021, **33**, 2105178.
- S6 X. Han, J. Z. Chen, M. F. Chen, W. J. Zhou, X. Y. Zhou, G. W. Wang, C. P. Wong, B. Liu, L. S. Luo, S. Y. Chen, S. Q. Shi, Induction of planar Li growth with designed interphases for dendrite-free Li metal anodes, *Energy Storage Mater.*,

2021, **39**, 250-258.

- S7 Z. D. Hao, Y. Wu, Q. Zhao, J. D. Tang, Q. Q. Zhang, X. X. Ke, J. B. Liu, Y. H. Jin, H. Wang, Functional separators regulating ion transport enabled by metal-organic frameworks for dendrite-free lithium metal anodes, *Adv. Funct. Mater.*, 2021, **31**, 2102938.
- S8 X. Chen, R. Y. Zhang, R. R. Zhao, X. Q. Qi, K. J. Li, Q. Sun, M. Y. Ma, L. Qie, Y. H. Huang, A “dendrite-eating” separator for high-areal-capacity lithium-metal batteries, *Energy Storage Mater.*, 2020, **31**, 181-186.
- S9 C. Ma, Y. M. Feng, X. J. Liu, Y. Yang, L. J. Zhou, L. B. Chen, C. L. Yan, W. F. Wei, Dual-engineered separator for highly robust, all-climate lithium-sulfur batteries, *Energy Storage Mater.*, 2020, **32**, 46-54.
- S10 Z. Luo, C. Liu, Y. Tian, Y. Zhang, Y. L. Jiang, J. H. Hu, H. S. Hou, G. Q. Zou, X. B. Ji, Dendrite-free lithium metal anode with lithophilic interphase from hierarchical frameworks by tuned nucleation, *Energy Storage Mater.*, 2020, **27**, 124-132.
- S11 Q. Lei, Q. Zhang, X. Wu, X. Wei, J. Zhang, K. Wang, J. Chen, Towards ultra-stable lithium metal batteries: Interfacial ionic flux regulated through LiAl LDH-modified polypropylene separator, *Chem. Eng. J.*, 2020, **395**, 125187.
- S12 L. Yang, L. Sheng, X. Gao, X. Xie, Y. Bai, G. Liu, H. Dong, T. Wang, X. Huang, J. He, rGO/Li-Al-LDH composite nanosheets modified commercial polypropylene (PP) separator to suppress lithium dendrites for lithium metal battery, *Electrochim. Acta*, 2022, **430**, 141073.